

DOI: 10.1002/adfm.200701105

The Very Low Shear Modulus of Multi-Walled Carbon Nanotubes Determined Simultaneously with the Axial Young's Modulus via *in situ* Experiments**

By Xian-Long Wei, Yang Liu, Qing Chen,* Ming-Sheng Wang, and Lian-Mao Peng

The natural frequencies (f) as a function of the length (L) of single multi-walled carbon nanotubes (CNTs) are measured using the electric-field-induced resonance method together with the “nanoknife” technique for cutting nanotubes to the desired length. The experimental f - L data for short CNTs are found to be adequately described by the Timoshenko beam model, but not by the widely-used Euler-Bernoulli beam model. The failure of the Euler-Bernoulli beam model is due to its neglect of the significant effect of shear deformation caused by the extremely-anisotropic mechanical properties of CNTs. The axial Young's modulus and radial shear modulus of CNTs are obtained simultaneously through fitting the experimental f - L data with the Timoshenko beam model.

1. Introduction

Due to their outstanding mechanical properties, carbon nanotubes (CNTs) have been found to be promising in such applications as nanocomposites, probe-microscopy tips, nanoresonators, etc. Having a quasi-one-dimensional nanostructure, CNTs also provide an ideal system for the study of vibration theory and wave propagations in low-dimensional systems. The axial Young's modulus of CNTs has been measured through thermal vibration,^[1] electric-field-induced resonance,^[2] tensile-loading experiments inside a scanning electron microscope (SEM)^[3] and atomic force microscopy (AFM) experiments.^[4] A novel method has recently been developed to precisely measure the Young's modulus of single-walled CNTs (SWCNTs) by studying the diameter dependence of the buckling wavelengths of the SWCNTs on elastomeric substrates.^[5] Of all the available methods, the electric-field-induced resonance method is widely used to study the mechanical properties of nanomaterials, including nanotubes,^[2,6-9] nanowires^[10] and nanobelts.^[11] In carrying out resonance experiments, carbon nanotubes or other nanowires are fixed at one end or at both ends. Resonance vibration is induced by an external electric field. The natural frequencies, length and diameters of the CNTs or nanowires are measured and the Young's modulus is deduced using continuum theory.

All of the papers published so far use the Euler-Bernoulli beam model^[12] to deduce the Young's modulus of the CNT from the natural frequency. Although widely used, the Euler-Bernoulli beam model of flexural motions of elastic beams is “the simple-beam theory”, ignoring rotatory inertia and shear-deformation effects. Theoretical studies show that when the vibration frequency is in THz range and when the length-to-diameter ratio is small, the Timoshenko beam model, which also includes rotation and shear deformation, should be used.^[13,14] In the mean time, different models have been developed in the last ten years based on continuum or molecular mechanics for estimating the elastic properties of nanotubes.^[15-19] On the other hand, almost all of the previous experimental works deduced the Young's modulus of CNTs based on single-point measurements, while in principle it is much more reliable to measure the natural frequencies from the same nanotube but at different lengths. To the best of our knowledge, so far, there is not an experimental work validating the Euler-Bernoulli beam model or continuum theories for analyzing the vibration of CNTs, nor is there a single set of experimental data analyzed using the Timoshenko beam model.

Recently, we developed a method to cut CNTs to the desired length using a “nanoknife”.^[20] In the present work, we measure the natural frequencies (f) of the first flexural mode of individual CNTs at different lengths (L) using the “nanoknife” technique and the electric-field-induced resonance method. The measured f - L data allow us to verify whether or not the Euler-Bernoulli beam model is adequate to analyze the flexural vibrations of a CNT. We find that the experimental f - L data deviate from the Euler-Bernoulli beam model significantly for short CNTs and, in general, the Timoshenko beam model is needed to fully describe the flexural vibration of

[*] Prof. Q. Chen, X.-L. Wei, Y. Liu, Dr. M.-S. Wang, Prof. L.-M. Peng
Key Laboratory for the Physics and Chemistry of Nanodevices and
Department of Electronics
Peking University, Beijing 100871, (P.R. China)
E-mail: qingchen@pku.edu.cn

[**] We thank Prof. Jin Zhang for the CNT samples. This work was supported by the NSF of China (60771005, 60728102, 60571002) and the MOST (2006CB932401).

a CNT. A significant shear-deformation effect due to the extremely-anisotropic mechanical properties of CNTs is observed. We also obtain simultaneously the axial Young's modulus and radial shear modulus of the CNTs through fitting the f - L data with the Timoshenko beam model.

2. Results and Discussion

2.1. Theory Background

The Euler-Bernoulli beam model has been widely used to deduce the Young's modulus of CNTs from their natural frequency, measured through electric-field-induced resonance experiments.^[2] According to the Euler-Bernoulli beam model, the natural frequency of the i th flexural mode of a cylinder can be expressed as:^[12]

$$f_i = \frac{\beta_i^2}{8\pi L^2} \sqrt{\frac{(D_o^2 + D_i^2)E}{\rho}} \quad (1)$$

In Equation 1, β_i are constants with $\beta_1 = 1.875$, $\beta_2 = 4.694$, $\beta_3 = 7.855$, etc.; L is the length and D_o and D_i are the outer and inner diameters of the cylinder (in our case the CNT); E is the axial Young's modulus and $\rho = 2.1 \text{ g cm}^{-3}$ ^[9] is the mass density per unit volume. With known D_o , D_i and L , which can be directly measured using transmission electron microscopy (TEM) and/or scanning electron microscopy (SEM), the Young's modulus of a CNT can be calculated using Equation 1, from f_i measured in resonance experiments.

Although the Euler-Bernoulli beam model is widely used, it assumes that the rotation of the element is insignificant compared to the vertical translation, and the shear deformation is small compared with the bending deformation. Therefore, the theory is valid if the length-to-diameter ratio is relatively large (e.g., more than 10), and if the beam does not become too "wrinkled" because of flexure.^[12] A carbon nanotube is an anisotropic material. The radial shear modulus of SWCNT ropes^[4] and multi-walled CNTs (MWCNTs)^[21] has been found to be of the order of 1 GPa by bending the CNTs on special porous substrates using AFM, while the axis Young's modulus of the CNTs is of the order of 1 TPa.^[4,21] The anisotropic mechanical properties of the CNT may make the Euler-Bernoulli beam model inadequate. On the other hand, the more-accurate Timoshenko beam model considers not only the translatory motion of the elements but also rotation and shear deformation.

According to the Timoshenko beam model:^[22]

$$EI \frac{\partial^4 y}{\partial x^4} + \rho A \frac{\partial^2 y}{\partial t^2} - \rho I \frac{\partial^4 y}{\partial x^2 \partial t^2} - \frac{\rho I E}{\kappa G} \frac{\partial^4 y}{\partial x^2 \partial t^2} + \frac{\rho^2 I}{\kappa G} \frac{\partial^4 y}{\partial t^4} = 0 \quad (2)$$

In Equation 2, E is the axial Young's modulus; $\rho = 2.1 \text{ g cm}^{-3}$ ^[9] is the mass density of the CNT per unit volume; y is the transverse displacement; x is the axial coordinate; t is the time;

G is the radial shear modulus; I is the cross-sectional area moment of inertia; A is the cross-sectional area and κ is the shear coefficient. The third term from the left in Equation 2 is the term of rotation. The last two terms are due to shear deformation. These two terms become zero for infinite G . Neglecting the terms of rotation and shear deformation, Equation 2 reduces to the Euler-Bernoulli beam model. In our experiments, the CNTs were clamped at W tips at one end and free at the other end. Applying this boundary condition, the following equation can be obtained:^[23]

$$2 + [b^2(r^2 - s^2)^2 + 2] \cosh(b\alpha) \cos(b\beta) - \frac{b(r^2 + s^2)}{(1 - b^2 r^2 s^2)^{\frac{1}{2}}} \sinh(b\alpha) \sin(b\beta) = 0 \quad (3)$$

In equation 3, $b = \left(\frac{4\pi^2 \rho A L^4 f^2}{EI}\right)^{\frac{1}{2}}$, $r = \left(\frac{1}{AL^2}\right)^{\frac{1}{2}}$, $s = \left(\frac{EI}{\kappa A G L^2}\right)^{\frac{1}{2}}$, $\alpha = \frac{1}{\sqrt{2}} \{[(r^2 - s^2)^2 + \frac{4}{b^2}]^{\frac{1}{2}} - (r^2 + s^2)\}^{\frac{1}{2}}$, $\beta = \frac{1}{\sqrt{2}} \{[(r^2 - s^2)^2 + \frac{4}{b^2}]^{\frac{1}{2}} + (r^2 + s^2)\}^{\frac{1}{2}}$ and f is the natural frequency. The shear coefficient κ describes the ratio of the average shear strain on a section to the shear strain at the centroid and relates to the cross-sectional shape of the beams. For hollow circular CNTs, $\kappa = 6(1 + \nu)(1 + m^2)^2 / ((7 + 6\nu)(1 + m^2)^2 + (20 + 12\nu)m^2)$,^[24] where $m = D_i / D_o$ and $\nu = 0.012$ is the Poisson ratio, which is assumed to be equal to the Poisson ratio of compression-annealed pyrolytic graphite, perpendicular to the basal plane.^[25]

2.2. Experimental and Fitting Results

Figure 1a depicts the setup of our experiments. Figure 1(b-d) are SEM images showing the first-mode resonance of the same CNT but at different lengths. More than ten CNTs were studied and ten complete sets of f - L data were obtained. Two typical sets of f - L data are shown in Figure 2(a-b). The error in the measurement of f is less than 0.5%, which is estimated from the dependence of the resonance amplitude on the frequency. The error in the measurement of L (indicated by the error bars in Fig. 2) contains contributions from two sources. The length, measured from the SEM images, has an accuracy better than 20 nm in the magnification range we used, which corresponds to an error of much less than 1% for most of the values of L that we measured. The error caused by the tilting of the CNTs from the horizontal plane is estimated to be smaller than 3% if we consider the tilting angle is less than 15°.

If the Euler-Bernoulli beam model is adequate for CNTs, the f - L data obtained from the same CNT should be able to be fitted by Equation 1. Compared with the one-point measurements, fitting of the f - L data gives a much-more-reliable value for the Young's modulus. The data points shown in Figure 2(a-b) are two typical sets of experimental f - L data obtained from two CNTs. The f - L data shown in Figure 2a can be fitted well with the Euler-Bernoulli beam model and $E = 520 \text{ GPa}$ was obtained. However, the f - L data shown in Figure 2b, which

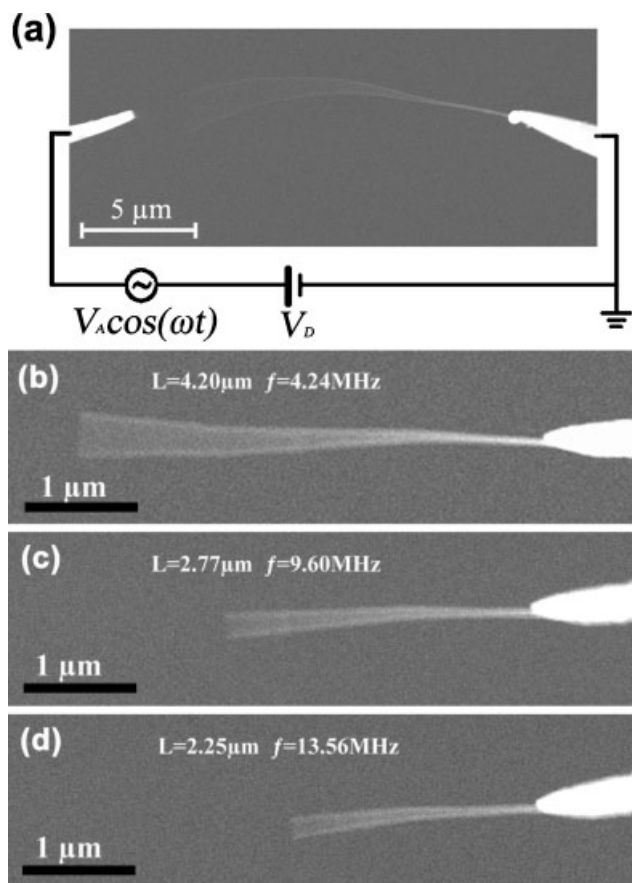


Figure 1. a) Diagram showing the setup of our experiments. b, c) and d) are SEM images showing the first-mode flexural resonance of the same CNT but with different lengths.

are obtained from a shorter CNT, cannot be adequately fitted with the Euler-Bernoulli beam model. Our results obtained from more than ten CNTs show that the Euler-Bernoulli beam model does not fit the experimental f - L data well when the CNTs are shorter than several micrometers.

Solving Equation 3 numerically, we found that our experimental f - L data can be fitted using the Timoshenko beam model and E and G of the CNTs can be obtained simultaneously through the fitting. The dotted lines in Figure 2 are the least-square fitting of the f - L data based on the Timoshenko beam model. Although not fitted well using the Euler-Bernoulli beam model, the f - L data shown in Figure 2b can be fitted well using the Timoshenko beam model, indicating that the effects of rotary inertia and shear deformation are significant for short CNTs. The f - L data measured from long CNTs, like those shown in Figure 2a, can be fitted well with both the Timoshenko beam model and the Euler-Bernoulli beam model. The fitting curves based on the two models overlap in Figure 2a and the same value of E is obtained, indicating the effect of rotary inertia and shear deformation is insignificant in that length range. In the case shown in Figure 2a, only E can be obtained from fitting data

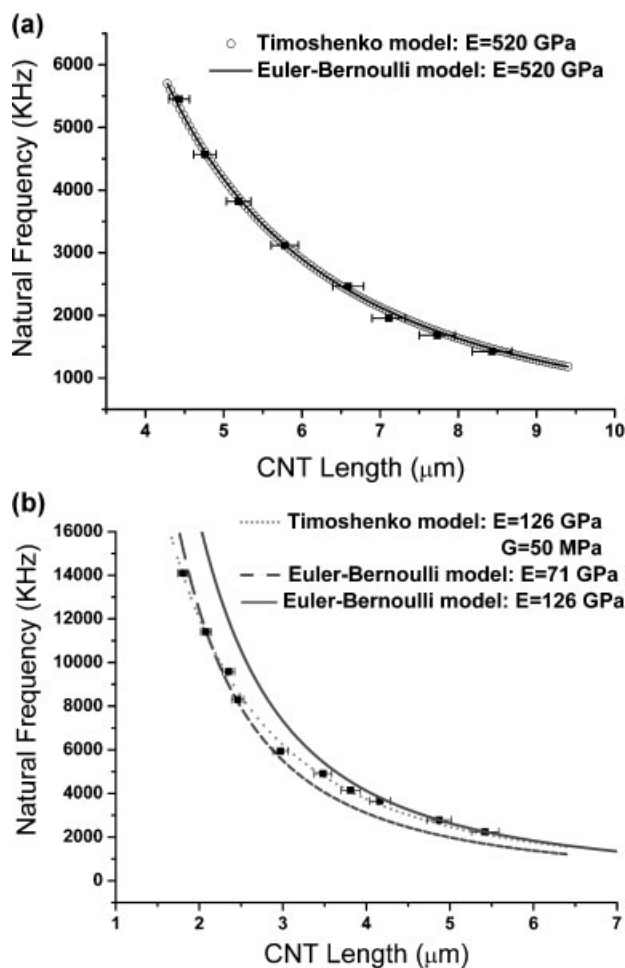


Figure 2. Two typical sets of experimental f - L data obtained from two CNTs ((a) and (b) correspond to CNT 9 and 6 in Table 1). The broken line is the least-square fitting with the Euler-Bernoulli beam model, while the dotted lines are the least-square fitting with the Timoshenko beam model. The full line in (b) is the plot for $E = 126$ GPa using the Euler-Bernoulli beam model. The E and G obtained from the fittings are indicated in each figure.

with the Timoshenko beam model due to the large error in fitting for G . In the case shown in Figure 2b, not only a large fitting error exists when we fit the f - L data with the Euler-Bernoulli beam model, but also the value of E obtained from the Euler-Bernoulli beam model is smaller than that obtained from the Timoshenko beam model. Table 1 summarizes our results obtained from ten CNTs with complete sets of f - L data. The fitting was realized by changing f at a fixed L . The standard deviation of f was set to be $0.03f$ to include the measurement error of L , although the measurement error of f is less than 0.5%. The Young's modulus (E) obtained from the Timoshenko beam model ranges from 126 GPa to 937 GPa, with an average value of 470 GPa. Six out of eight of the CNTs have a value for G of several hundred MPa, which is at least three orders of magnitude smaller than the value of E . Samples 1 and 6 have an even lower value for G of less than 100 MPa.

Table 1. Summary of results obtained from ten CNTs with complete sets of f - L data. The errors for E and G were calculated from the square root of the diagonal elements of the covariance matrix. The standard deviation of f was set to be $0.03 f$. The diameters D_o and D_i were measured using TEM, except for the samples marked with “*”, whose D_o was measured using SEM and D_i was assumed because the samples were lost during transfer from SEM to TEM.

CNT samples	D_o [nm]	D_i [nm]	Length range measured [μm]	E from Euler model [GPa]	E from Timoshenko model [GPa]	G from Timoshenko model [MPa]
1	30	7.9	2.30–6.48	304	603 ± 32	33 ± 3
2*	45	8	3.51–9.72	843	937 ± 36	401 ± 207
3	55.3	12	2.28–11.9	250	304 ± 8	241 ± 51
4	56.8	9.9	2.88–9.72	452	483 ± 15	785 ± 554
5	56.9	12.4	2.38–16.1	449	574 ± 15	364 ± 76
6*	60	10	1.80–5.42	71	126 ± 6	50 ± 5
7	60.1	9.1	4.13–12.8	368	434 ± 16	137 ± 42
8*	65	10	3.73–8.20	334	391 ± 22	204 ± 98
9	46.5	9.3	4.43–8.43	520	520 ± 14	–
10	60.9	9.2	2.56–18.4	344	350 ± 7	–

2.3. Discussion

While in this work, values for E and G of CNTs are obtained simultaneously without assuming any unknown parameters, previously, the radial shear modulus of CNTs has only been measured by bending CNTs on special porous substrates using AFM.^[4,21] Because only the outer diameter of the CNT can be measured by AFM, the inner diameter had to be ignored or assumed to obtain the radial shear modulus of SWCNT ropes^[4] and MWCNTs,^[21] even though the results are sensitive to the assumption of the inner diameter of CNTs. The Young’s modulus was also assumed to be 600 GPa to determine the shear modulus of SWCNT ropes.^[4] Another shortcoming of these AFM works is that the CNTs deposited on porous substrates may not be well anchored to the substrate, although a clamped model was assumed,^[4,21] while the boundary conditions of the CNTs in our experiments are firmly ensured by clamping the CNTs at the top tip of W probes with deposited amorphous carbon.

As shown in Table 1, the values of E and G are spread in a relatively-large range. Such data scattering is not due to the errors in our experiments, but originates from the different structures (especially defect structures) of the CNTs. The measurement error of the diameters in our experiments is less than 5%. The 5% error in D_o causes an error of less than 10% in the value of E and an error of less than 2% in the value of G . The 5% error in D_i causes an error of less than 2% in both E and G . Even considering the guessed inner diameters of CNT 2, 6, and 8, the errors in E and G introduced by the errors in D_i and D_o will not be larger than 15%. The errors caused by the measurements of f and L have been included in the fitting error, as shown in Table 1. Therefore, the errors in the experiments are not responsible for the large scattering of E and G . A large scattering of E has been reported for SWCNTs, mainly attributed to a different choice of the thickness.^[26] However, the thickness of the MWCNTs is the thickness of the whole MWCNTs, and is obtained from $t = r_o - r_i$ (where r_o and r_i are the radii of the outmost and innermost shells), and thus the Young’s modulus correlates little to the choice of the

thickness of a single shell, especially for the thick MWCNTs we studied. On the other hand, the structure of the CNTs does vary for different individual CNT. Unlike in the case of growing bulk crystals, it has been almost impossible so far to grow CNTs with the same structure, for example having the same diameter, the same chirality and the same defects. Although the CNTs we measured were synthesized through chemical vapor deposition (CVD) in one run and located in the same area on the same substrate, the structures of the CNTs are not all the same. The inner diameter of the present CNTs is around 10 nm, but the outer diameter ranges from 30 nm to 65 nm. As illustrated by TEM observations, some CNTs have nearly-perfect shell structures (as shown in Fig. 3a), while others may have severe defects (like that shown in Fig. 3b), although most of our CNT samples are like that shown in Figure 4a, and have a good shell structure with some defects on the wall.

So far, more than ten groups have measured the Young’s modulus of CNTs experimentally using different methods. The results show that E of arc-discharge MWCNTs is larger than E of CVD MWCNTs. The Young’s modulus of arc-discharge MWCNTs was measured to be 670–1100 GPa while the Young’s modulus of catalytic MWCNTs was 12–50 GPa.^[27]

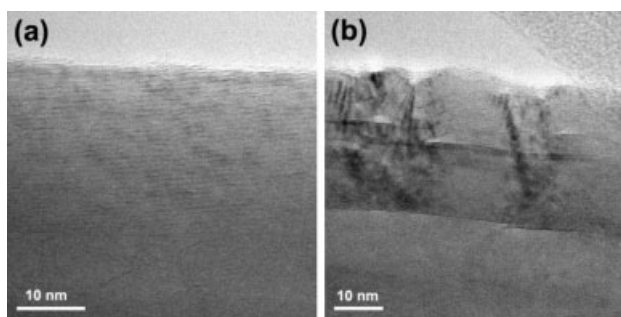


Figure 3. High-resolution TEM images taken from (a) a CNT with a good wall structure and (b) a CNT with severe defects.

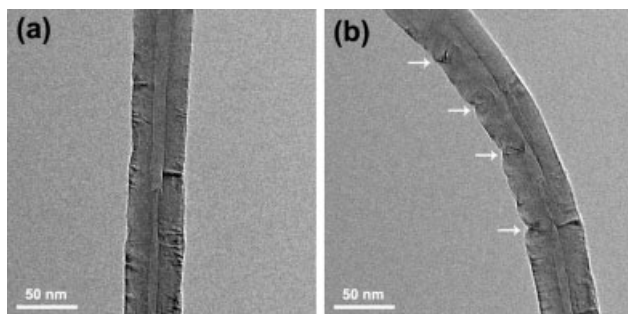


Figure 4. TEM images taken (a) before and (b) after a CNT was bent. As indicated by the arrows, several deep buckles appeared and developed gradually on the inner arc of the bent CNTs when the curvature of the CNT increased.

The Young's modulus of CNTs is also sensitive to the wall defects and is smaller for CNTs with more defects.^[7] The Young's modulus obtained from CVD MWCNTs ranges from 3 GPa for CNTs with many defects to 300 GPa for CNT with fewer defects.^[6,7,21,27] A different degree of imperfection in SWCNT ropes also makes their shear modulus spread in a wide range from 0.7 GPa to 6.5 GPa.^[4] These facts indicate that, not only do the CNTs synthesized by different methods exhibit quite different values of the Young's modulus, but the CNTs synthesized by the same method also show widely scattered values of the Young's modulus. In the present work, among the ten CNTs from which we obtained the complete f - L data sets, eight of the CNTs have a value for E in the range of 300 to 600 GPa, indicating the present CNTs have good wall structures, which is consistent with our TEM observation. The present, measured E value is also comparable with that of arc-discharge MWCNTs with similar diameters,^[1-3] indicating good CVD MWCNTs can be as strong as arc-discharge MWCNTs.

The shear modulus, G , of most of our CNT samples has a value of several hundred MPa (except samples 1 and 6, which have even smaller G). This G value is smaller than has been previously reported for MWCNTs (1.4 GPa),^[21] SWCNTs ropes (from 6.5 GPa to 0.7 GPa),^[4] and the shear modulus (c_{44}) of single-crystal graphite (4.5 GPa), but is of the same order as the shear modulus of compression-annealed pyrolytic graphite (0.18 GPa).^[25] The shear modulus (G) of an MWCNT is supposed to be dominated by the shear between shells^[21] and is sensitive to the interaction of shells. The low shear modulus of compression-annealed pyrolytic graphite has been reported to be due to the presence of very-mobile dislocations in the basal plane.^[25] Mobile dislocations may also be the cause of the low shear modulus of our CNT samples. The very-low G of samples 1 and 6 may be due to severe defects on the wall. We occasionally observed CNTs that had severe defects, with some shells being seriously wrinkled, leaving free space between the shells (as shown in Fig. 3b). Such defects may reduce the interaction between shells so that the shells become more sliding. Such defects may be responsible for the extremely-low

G of samples 1 and 6. As the defect conditions vary for different CNTs, which is reasonable for CVD-grown CNTs, it is understandable that G is different for different CNTs.

Our results show no obvious relation between E (or G) and the outer diameter of the CNT in the diameter range in which we performed our measurements (from 30 nm to 65 nm). In the literature, some reports show no obvious relation between the outer diameter (d) of the CNT and E ,^[1,3,6,28] while other people found E to decrease sharply with increasing d .^[2] We noticed that in ref.^[2], E starts to increase when d is smaller than 20 nm, while for d larger than 20 nm, there is not much change of E with d . Therefore, our result has no disagreement with the literature. In fact, in the present case, as the inner diameter of the CNTs is roughly the same, around 10 nm, the change of the outer diameter also means a change of the wall thickness. Similar things also happened in most of the previous works. Further work is needed to separate the effect of thickness and the outer diameter of the CNTs.

Periodic wave-like distortions of the inner arc of bent MWCNTs have been observed by TEM and have been thought to be the reason for the decrease of E from about 1 to 0.1 TPa when the CNT diameter increased.^[2] To observe the structural change of the CNT during deformation, we also performed bending experiments in TEM. Figure 4 shows the TEM images of the same CNT taken before and after bending. Figure 4a shows that our CNTs are straight, and have an internal hollow space and a uniform diameter. The wall is highly crystalline, but contains some defects, which is common for CVD-grown CNTs. We did not observe any periodic wave-like distortions. Instead, a gradual buckling^[29] was seen at several discrete sites on the inner arc of the bent CNT (indicated by the arrows in Fig. 4b). Periodic wave-like distortions are supposed to be the distinctive feature of thick MWCNTs without internal hollow spaces like that shown in ref.^[2], because the outer tubes are constrained by the inner tubes and deep buckles do not have space to develop.^[16] However, the large, hollow space in our CNT samples makes them tend to be deeply buckled at both the outer and inner shells when the CNTs are bent. Due to the thick walls of the CNTs, the critical buckling curvature of the outer shells deviates much from that of the inner shells, so different shells buckle at different curvatures and the buckling of the whole CNT happened gradually.^[29] Without periodic wavelike distortions, our CNT samples can retain a large Young's modulus (about 0.5 TPa) with a large diameter (around 50 nm). Therefore, hollowed MWCNTs are more preferable for mechanical applications because they can retain a larger bending modulus than solid ones.

For normal isotropic materials, G has the same order as E , related by $G = \frac{E}{2(1+\nu)}$, where ν is Poisson's ratio. However, the present results show that G of a typical CNT is about 3–4 orders of magnitude smaller than E , and there is no obvious correlation between E and G , which is contrary to normal isotropic materials. The main reason is that the CNTs have extremely-anisotropic mechanical properties. The different dependence of E and G on the defects may also be one of the reasons. All types of defects are supposed to decrease the

Young's modulus, while the shear modulus can be increased or decreased by defects. For example, the misalignment of the graphitic planes with the tube axis has been shown to be the main reason for the reduction of the Young's modulus of catalytic CNTs, but increases the shear modulus because shear deformations can be blocked by disorder in the graphitic-plane stacking.^[27] On the other hand, for the CNT shown in Figure 3b, the Young's modulus will be decreased due to the seriously-wrinkled shells and the shear modulus will also be decreased due to the free space between the shells.

2.4. Calculations and Analysis

To further understand the effects of rotary inertia and shear deformation on the flexural vibrations of CNTs, we performed numerical analysis. With given values of E and G , f - L curves were calculated using the Euler-Bernoulli beam model (using Eq. 1) and the Timoshenko beam model (using Eq. 3). A tubular beam was assumed to have an outer diameter of 60 nm and an inner diameter of 10 nm in our calculations. In the calculation, $E = 500$ GPa was used, considering the average, measured E in the present work is 470 GPa. Figure 5a shows the calculated results for the first flexural mode. It shows that the deviation of the Euler-Bernoulli beam model from the Timoshenko beam model is more significant for lower G . The deviation happens at a length of less than $0.3 \mu\text{m}$ if $G = 200$ GPa, while the deviation is significant at a length of $5 \mu\text{m}$ if $G = 0.05$ GPa. When G is large, the deviation between the two models is mainly due to the effect of rotary inertia, as G only relates to the terms of shear deformation. When $G = 200$ GPa, the deviation between the two models is negligible until the length is less than $0.3 \mu\text{m}$, indicating the rotary inertia is not significant until the length-to-diameter ratio is less than 5. Therefore, the deviation of the f - L data from the Euler-Bernoulli beam model at long lengths in Figure 2b is mainly caused by the significant effect of shear deformation due to the very-low shear modulus. For normal isotropic materials, G has the same order as E , the effect of shear deformation is negligible and the Euler-Bernoulli beam model is valid if the length-to-diameter ratio is more than 10.^[12] However, the present results show that G of a typical CNT is about 3–4 orders of magnitude smaller than E . The extremely-anisotropic mechanical properties of the CNT makes the effect of shear deformation significant and the Euler-Bernoulli beam model inadequate for the vibrations of the CNT, even though the length-to-diameter ratio is much larger than 10.

We also calculated f - L curves for different modes with $G = 1$ GPa and $E = 500$ GPa. Figure 5b shows the results. The effect of shear deformation is more significant for higher modes. For the first mode, it becomes significant when the length is about $2 \mu\text{m}$. For the second and third modes, the effect of shear deformation becomes significant at lengths of about $5 \mu\text{m}$ and $7 \mu\text{m}$, corresponding to a length-to-diameter ratio of about 100. Therefore, the Euler-Bernoulli beam model can be

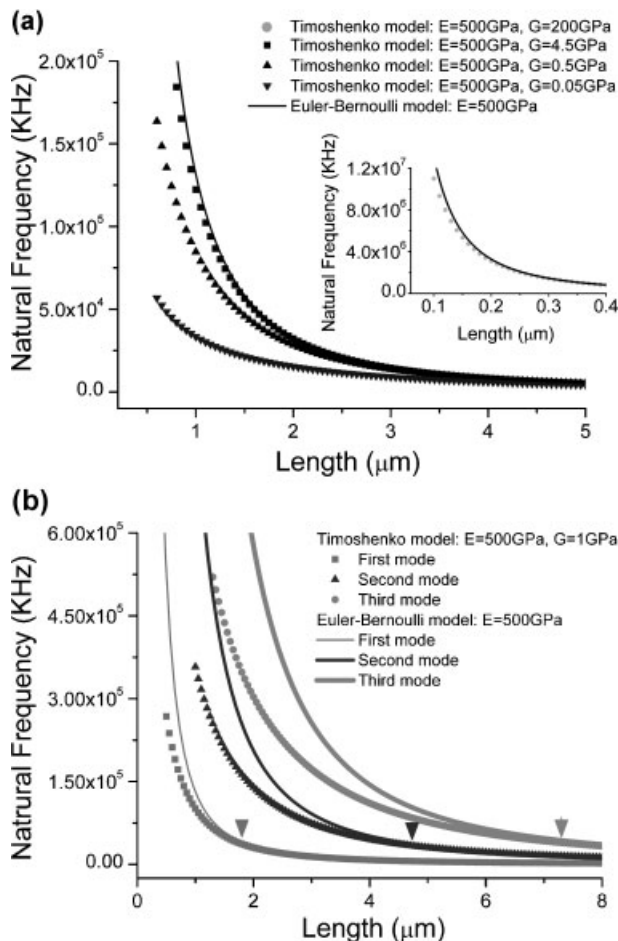


Figure 5. Calculated f - L curves from Equation 1 (full curves) and Equation 3 (dashed or dotted curves) for given E and G . a) shows f - L curves of the first mode for different G when $E = 500$ GPa. The inset in (a) shows the f - L curves for $G = 200$ GPa. The black, full curves in (a) are calculated from Equation 1 for $E = 500$ GPa. b) shows f - L curves of different modes when $E = 500$ GPa and $G = 1$ GPa. The arrows indicate the length when f calculated from the two models deviates by 10%.

used to describe the vibration of a CNT at low modes when the length-to-diameter ratio of the CNT is larger than about 100. The exact value of the length-to-diameter ratio, beyond which the Euler beam theory can be used, is determined by the Young's modulus, the shear modulus of the CNTs and the modes of the vibration.

For CNTs with specific E , G and length, the natural frequencies calculated from the Euler-Bernoulli beam model are higher than those calculated from the Timoshenko beam model if the effect of shear deformation is significant (Fig. 5). The significant effect of shear deformation results in the natural frequencies of the CNT not increasing as quickly as described by the Euler-Bernoulli beam model when the length decreases. This effect should be considered when ultrahigh-frequency CNT resonators are designed.^[30] On the other hand, for a given natural frequency, E calculated using the Euler-Bernoulli beam model will be lower than that calculated

using the Timoshenko beam model, which means E is underestimated using the Euler-Bernoulli beam model.

The present success in fitting experimental f - L data with the Timoshenko beam model indicates continuum beam theory is still applicable for MWCNTs and can provide valuable information on their mechanical properties. For SWCNTs and CNTs with few walls, experimental results are needed to validate whether or not more-advanced theories based on continuum or molecular mechanics^[15-19] are needed.

3. Conclusions

In conclusion, we describe a method for measuring the natural frequencies (f) as a function of the length (L) of individual CNTs, combining the electric-field-induced resonance method and the “nanoknife” technique. Through fitting the experimental f - L data, we find that flexural vibrations of MWCNTs deviate significantly from the widely-used Euler-Bernoulli beam model when the length of the CNT is shorter than several micrometers. Our results show that the Timoshenko beam model is needed to fully describe the flexural vibrations of the CNT. The axial Young's modulus (E) and radial shear modulus (G) of the CNTs are obtained simultaneously through fitting the experimental f - L data using the Timoshenko beam model. The shear modulus G is found to be of the order of several hundred MPa, which is 3–4 orders of magnitude smaller than E , indicating CNTs have extremely-anisotropic mechanical properties. Our results show that the significant effect of shear deformation, caused by the extremely-anisotropic mechanical properties of the CNTs is the reason that the flexural vibration of the CNTs deviates from the Euler-Bernoulli beam model. The present method is also useful to simultaneously measure the axial Young's modulus and the radial shear modulus of other nanotubes and nanowires. The extremely-anisotropic mechanical properties may be a common feature for nanotubes with a layered structure.

4. Experimental

Our experiments were performed inside a scanning electron microscope (FEI XL 30F) using a nanoprobe system (Kleindiek). MWCNTs synthesized using the CVD method were transferred into the SEM through a Pt tip [20]. Under observation with SEM, a long and straight CNT protruding from the Pt tip was selected, a W tip was manipulated to contact the selected CNT by the van der Waals interaction and align well. Amorphous carbon was then deposited on the connecting area using electron-beam-induced deposition to clamp the CNT firmly at the top end of the W tip. The CNT was then separated from the Pt tip through an electrical current. The length of the CNT was adjusted using the “nanoknife” technique [20] and was measured from SEM observations. Extra care was taken to set the W tip as horizontal as possible so that the CNTs were horizontal and the length measured from the SEM images was accurate. The second W tip was manipulated to be close to the free end of the CNT. Both a DC voltage (V_D) and an AC voltage ($V_A \cos(\omega t)$) were applied to the second W tip through a signal generator (Agilent 33220A) to drive the CNT. The amplitude of the DC voltage was set to be 0–2 V (usually 0 V

to avoid tensioning CNTs by static electrical forces) and the amplitude of the AC voltage was set to be about 2–4 V. When the frequency of the alternating electrical force equals the natural frequencies of the CNT, the CNT will be resonant, which can be judged by the deflected contour. By examining whether the amplitude of the resonance changes linearly with V_D , the true natural frequencies of the CNTs are found from the frequency of the AC voltage [2]. Repeating the process of cutting the CNT to the desired length and then measuring the natural frequency, the relationship between the CNT's length (L) and natural frequency (f) for the individual CNTs was obtained. After finishing the SEM measurements, the CNT was then transferred to a transmission electron microscope (FEI Tecnai G20) by a nanoprobe system (Nanofactory) and the inner and outer diameters of the CNT were measured.

Received: September 25, 2007

Revised: February 5, 2008

- [1] M. M. J. Treacy, T. W. Ebbesen, J. M. Gibson, *Nature* **1996**, *381*, 678.
- [2] P. Poncharal, Z. L. Wang, D. Ugarte, W. A. de Heer, *Science* **1999**, *283*, 1513.
- [3] M. F. Yu, O. Lourie, M. J. Dyer, K. Moloni, T. F. Kelly, R. S. Ruoff, *Science* **2000**, *287*, 637.
- [4] J. P. Salvetat, G. A. D. Briggs, J. M. Bonard, R. R. Bacsa, A. J. Kulik, *Phys. Rev. Lett.* **1999**, *82*, 944.
- [5] D. Y. Khang, J. L. Xiao, C. Kocabas, S. MacLaren, T. Banks, H. Q. Jiang, Y. Huang, J. A. Rogers, *Nano Lett.* **2008**, *8*, 124.
- [6] R. P. Gao, Z. L. Wang, Z. G. Bai, W. A. de Heer, L. M. Dai, M. Gao, *Phys. Rev. Lett.* **2000**, *85*, 622.
- [7] J. Gaillard, M. Skove, A. M. Rao, *Appl. Phys. Lett.* **2005**, *86*, 233109.
- [8] P. Jaroenapibal, D. E. Luzzi, S. Evoy, S. Arepalli, *Appl. Phys. Lett.* **2004**, *85*, 4328.
- [9] R. Ciocan, J. Gaillard, M. Skove, A. M. Rao, *Nano Lett.* **2005**, *5*, 2389.
- [10] C. Q. Chen, Y. Shi, Y. S. Zhang, J. Zhu, Y. J. Yan, *Phys. Rev. Lett.* **2006**, *96*, 075505.
- [11] X. D. Bai, P. X. Gao, Z. L. Wang, E. G. Wang, *Appl. Phys. Lett.* **2003**, *82*, 4806.
- [12] L. Meirovitch, *Elements of Vibration Analysis*, 2nd Edition, McGraw-Hill, New York **1986**, p. 220.
- [13] Q. Wang, V. K. Varadan, *Int. J. Solids Struct.* **2006**, *43*, 254.
- [14] C. M. Wang, V. B. C. Tan, Y. Y. Zhang, *J. Sound Vib.* **2006**, *294*, 1060.
- [15] B. I. Yakobson, C. J. Brabec, J. Bernholc, *Phys. Rev. Lett.* **1996**, *76*, 2511.
- [16] M. Arroyo, T. Belytschko, *Phys. Rev. Lett.* **2003**, *91*, 215505.
- [17] L. F. Wang, Q. S. Zheng, J. Z. Liu, Q. Jiang, *Phys. Rev. Lett.* **2005**, *95*, 105501.
- [18] P. Zhang, Y. Huang, P. H. Geubelle, P. A. Klein, K. C. Hwang, *Int. J. Solids Struct.* **2002**, *39*, 3893.
- [19] J. Wu, K. C. Hwang, Y. Huang, *J. Mech. Phys. Solids.* **2008**, *56*, 279.
- [20] X. L. Wei, Q. Chen, Y. Liu, L. M. Peng, *Nanotechnology* **2007**, *18*, 185503.
- [21] G. Guhados, W. K. Wan, X. L. Sun, J. L. Hutter, *J. Appl. Phys.* **2007**, *101*, 033514.
- [22] S. Timoshenko, D. H. Young, W. Weaver, *Vibration Problems in Engineering*, 4th Edition, John Wiley & Sons, New York **1974**, p. 432.
- [23] T. C. Huang, *J. Appl. Mech.* **1961**, *28*, 579.
- [24] G. R. Cowper, *J. Appl. Mech.* **1966**, *33*, 335.
- [25] O. L. Blakslee, D. G. Proctor, E. J. Seldin, G. B. Spence, T. Weng, *J. Appl. Phys.* **1970**, *41*, 3373.
- [26] Y. Huang, J. Wu, K. C. Hwang, *Phys. Rev. B* **2006**, *74*, 245413.

- [27] J. P. Salvetat, A. J. Kulik, J. M. Bonard, G. A. D. Briggs, T. Stockli, K. Metenier, S. Bonnamy, F. Beguin, N. A. Burnham, L. Forro, *Adv. Mater.* **1999**, *11*, 161.
- [28] E. W. Wong, P. E. Sheehan, C. M. Lieber, *Science* **1997**, *277*, 1971.
- [29] X. J. Duan, C. Tang, J. Zhang, W. L. Guo, Z. F. Liu, *Nano Lett.* **2007**, *7*, 143.
- [30] H. B. Peng, C. W. Chang, S. Aloni, T. D. Yuzvinsky, A. Zettl, *Phys. Rev. Lett.* **2006**, *97*, 087203.
-